Influence of surface conductivity on the apparent zeta potential of TiO2 nanoparticles: application to the modeling of their aggregation kinetics

Izzeddine Sameut-Bouhaik, Philippe Leroy, Patrick Ollivier, Mohamed Azaroual, Lionel Mercury

Influence of surface conductivity on the apparent zeta potential of TiO_2 nanoparticles: application to the modeling of their aggregation kinetics

Izzeddine Sameut Bouhaik[1,2], Philippe Leroy[1*], Patrick Ollivier[1], Mohamed Azaroual[1], Lionel Mercury[2,3]

[1] BRGM, ISTO UMR 7327, 45060 Orléans, France

[2] Université d'Orléans, ISTO UMR 7327, 45071 Orléans, France

[3] CNRS/INSU, ISTO UMR 7327, 45071 Orléans, France

[*] Corresponding author and mailing address:

Philippe Leroy

BRGM

3 Avenue Claude Guillemin

45060 Orléans Cedex 2, France

E-mail: p.leroy@brgm.fr

Tel: +33 (0)2 38 64 39 73

Fax: +33 (0)2 38 64 37 19

Intended for publication in Journal of Colloid and Interface Science

Abstract

Titanium dioxide nanoparticles (TiO_2 NPs) are extensively used in consumer products. The release of these NPs into aquatic environments raises the question of their possible risks to the environment and human health. The magnitude of the threat may depend on whether TiO_2 NPs are aggregated or dispersed. Currently, limited information is available on this subject. A new approach based on DLVO theory is proposed to describe aggregation kinetics of TiO_2 NPs in aqueous dispersions. It has the advantage of using zeta potentials directly calculated by an electrostatic surface complexation model whose parameters are calibrated by ab-initio calculations, crystallographic studies, potentiometric titration and electrophoretic mobility experiments. Indeed, the conversion of electrophoretic mobility measurements into zeta potentials is very complex for metal oxide nanoparticles. This is due to their very high surface electrical conductivity associated with the electromigration of counter and co-ions in their electrical double layer. Our model has only three adjustable parameters (the minimum separation distance between NPs, the Hamaker constant, and the effective interaction radius of the particle), and predicts very well the stability ratios of TiO_2 NPs measured at different pH values and over a broad range of ionic strengths (KCl aqueous solution). We found an effective interaction radius that is significantly smaller than the radius of the aggregate and corresponds to the radius of surface crystallites or small clusters of surface crystallites formed during synthesis of primary particles. Our results confirm that DLVO theory is relevant to predict aggregation kinetics of TiO_2 NPs if the double layer interaction energy is estimated accurately.

Keywords: stability ratio, TiO_2, nanoparticle, zeta potential, surface conductivity, extended Stern model, linear superposition approximation, Derjaguin approximation, surface element integration.

1. Introduction

A number of studies have recently focused on the transport and fate of nanoparticles (NPs) in porous media and their potential risk for the environment and human health [1-5]. However, their transport is very difficult to predict due to their very high surface reactivity and, notably, to their versatility between their aggregated and dispersed states. Modeling their reactivity and mobility in an aqueous environment is, therefore, challenging [3, 6, 7].

Titanium dioxide (TiO_2) NPs are used in many consumer products (e.g. catalysts, paints, coatings, soaps, cosmetics, and sunscreens [7-9]) because they have a very high specific surface area and a sorption capacity for ionic and nonionic species [10, 11]. Their application for soil remediation and water treatment shows great potential [12-14]. Their increasing use inevitably leads to their entering various environmental compartments and questions now arise concerning their mobility, fate and toxicity for humans and the environment.

Aggregation and deposition in porous media are the major processes controlling TiO_2 NPs transport [15]. Both processes are highly dependent on interaction energies between particles (aggregation), and between particles and the surrounding aquifer rock (deposition on the collector) [2, 16, 17]. The interaction forces between NPs and between the NPs and the collector are controlled by the intrinsic properties of NPs (chemical composition, size, and shape [2]) and by the intrinsic properties of the rock (chemical composition and surface roughness [16]). When immersed in an aqueous electrolyte, NPs and rock develop a surface charge (associated with the hydroxylation of their surface and specific ion adsorption) and an electrical double layer (EDL) to cancel it. EDLs around particles having similar chemical composition and crystal structure

have the same polarity and strength. As a result, when two particles draw near each other, the overlapping double layers create a repulsive double layer force. This double layer force between NPs (of similar chemical composition and crystal structure) and rock can be repulsive if the EDLs of both materials have the same polarity (which fosters aggregation), or attractive if the EDLs have opposite polarity (which fosters deposition) [6, 7, 17].

When NPs are repulsed from the rock surface, interaction energies between NPs greatly influence their aggregation [17]. TiO_2 NPs aggregate under specific chemical conditions (pH, ionic strength, the chemical nature of aqueous dissolved species) that reduce the repulsive double layer interaction energy between particles [10, 11]. Aggregation of TiO_2 NPs decreases their mobility in porous media and may even clog the porosity if their concentration in water is high. It may therefore enhance their deposition [7, 17]. However, their deposition can be reversible. Large quantities of TiO_2 NPs can be released into the environment if the pH of the pore water changes and moves away from the pH_{PZC} of TiO_2 NPs (PZC is the point of zero charge) or if the ionic strength of the pore water decreases to values below the critical coagulation concentration (CCC) [7, 16, 17]. It is, therefore, important to understand the aggregation of titanium dioxide NPs in water as a function of pH and ionic strength.

The double layer interaction energy is usually estimated using zeta potential data inferred from electrophoretic mobility measurements [10, 18]. However, because of their excess of electrical charges at the solid/water interface and very high surface-to-volume ratio, metal oxide NPs can have a very high surface electrical conductivity. This is associated with the electromigration of electrical charges in the double layer around the particle and is inversely proportional to the size of the particle [18-21]. Surface conductivity significantly decreases the magnitude of the electrophoretic mobility of

suspended particles when it is similar to or higher than the electrical conductivity of bulk water [18, 19], i.e. at low ionic strengths (typically lower than 10^{-1} M), and for pH values distant from the pH_{PZC} of the particle [18]. Under these physicochemical conditions, the intrinsic or true zeta potential of the NPs can be significantly underestimated if the zeta potential is not corrected for the retardation effect due to surface conductivity. Both the resulting repulsive interaction energy between double layers of particles and their stability ratios can therefore be underestimated.

Leroy et al. [18] recently developed a surface conductivity model for TiO_2 NPs immersed in a 1:1 aqueous electrolyte (KNO_3, $NaNO_3$, NaCl). In their work, surface conductivity of the Stern and diffuse layers are calculated by an electrostatic surface complexation model. Their electrokinetic transport model takes into account the retardation effect due to surface conductivity of elementary NPs on the electrophoretic mobility of the aggregate. Leroy et al. [18] adjusted the parameters of their extended Stern layer model (ESM) using both potentiometric titration and electrophoretic mobility experiments. Their corrected zeta potentials appear to be at least double the apparent zeta potentials estimated using the Smoluchowski equation. These authors also showed that potentiometric titration and electrophoretic mobility measurements of TiO_2 NPs can be predicted without the use of the unrealistic assumption of the presence of a stagnant diffuse layer at the TiO_2/water interface [8, 9].

Snoswell et al. [22] and Liu et al. [10] used the DLVO theory (constant charge approximation and linear superposition approximation, respectively) to correctly predict measured stability ratios of TiO_2 NPs immersed in a 1:1 aqueous electrolyte solution (KCl and NaCl, respectively). However, they used low apparent zeta potentials (not corrected for surface conductivity) and therefore predict low repulsive double layer interaction energy between particles. Snoswell et al. [22] found an unrealistically low

value of 2×10^{-20}J for the Hamaker constant of the TiO_2-H_2O-TiO_2 interface compared to values reported in the literature, which are between 4×10^{-20}J [23] and 9.4×10^{-20}J [24]. The predictions of Liu et al. [10] were only in quantitative agreement with the measured stability ratios of anatase NPs, which have two different sizes (mean radius of either 5 or 50 nm). The aggregation kinetics model of Liu et al. [10] underestimated stability ratios at low ionic strengths (2×10^{-3} M and 7×10^{-3} M NaCl for particles with a mean radius of 5 and 50 nm, respectively). Moreover, their measured stability ratios of anatase particles with a mean radius of 50 nm were not representative of stability ratios of pure TiO_2 NPs because their particles contained large quantities of impurities (silicon and phosphorous).

We provide here an aggregation kinetics model based on the DLVO theory and combined with a precise description of the electrochemical properties of the TiO_2 NPs/water interface (using an extended Stern model) that is valid regardless of the size of the NPs [18, 25]. The aggregation kinetics model uses true zeta potentials calculated directly by our electrostatic surface complexation model. The combined model is presented and tested against the stability ratios of pure TiO_2 NPs reported by Snoswell et al. [22] at different pH values and in a KCl solution.

2. Theoretical background

2.1. Aggregation kinetics models

In aggregating systems, the coagulation rate is usually expressed by the stability ratio, *W*, which is the ratio of the fast kinetic constant, k_f, to the slow kinetic constant, k_s [26]. The aggregation rate is rapid when all collisions result in aggregation in the absence of energy barriers, and slow in the presence of any repulsive energy barrier

(unfavorable conditions) that restricts aggregation to the primary minimum. The stability ratio of suspended particles in aqueous environments can be predicted using various DLVO and non-DVLO theories. The classic DLVO theory applies to smooth and spherical colloidal particles immersed in water [27, 28] through two types of interaction energies. The first is generally repulsive, due to the overlapping of the particles' EDLs and the second is attractive, due to London–van der Waals (VDW) interactions. However, NP aggregates have a more complex stability ratio than that of perfectly spherical and smooth colloidal particles, notably because of the discreteness of the surface charge [29, 30], the arising of relaxation processes [31-33], the presence of additional non-DLVO forces [34, 35], and the surface roughness of the particles [22, 36]. The classic DLVO theory frequently overestimates the experimental NP aggregation and deposition rates, probably by overlooking this complexity related to these well-known characteristics [22, 29, 37, 38].

Kallay et al. [39] combined an electrostatic surface complexation model (basic Stern model, BSM) and an aggregation model based on the DLVO theory to predict the stability ratios of anisotropic rutile particles (length of 170 ± 70 nm and width of 45 ± 10 nm) immersed in a 1:1 aqueous electrolyte (LiCl, KCl, CsCl). The parameters of their BSM were calibrated by crystallographic studies, potentiometric titration and electrophoretic mobility measurements. Their approach [39] allows direct estimation of the electrical potential at the outer Helmholtz plane (OHP). However, these authors used the constant potential assumption [40] to estimate interaction energies between particles and a too-simple equation to predict stability ratios. Indeed, this equation assumes that the stability ratio is approximately proportional to the exponential of the scaled maximum interaction energy. Additionally, Kallay et al. [39] did not compare their predictions to measured stability ratios.

Non-DLVO theories have recently been proposed to explain the weaker-than-expected stability of NP aggregates [41, 42]. Kallay and Zalac [41] consider that small NPs (radius < 5 nm) surrounded by a diffuse layer are similar to ions surrounded by their ion clouds because their size is small compared to the thickness of the electric double layer. In their aggregation kinetics model, therefore, NPs interact like two interacting ions sharing a common ion cloud. However, their model is only valid for NPs whose size is a few nanometers. Furthermore, their model, which assumes that NPs are like hydrated ions, is not realistic because NPs are an assemblage of atoms and molecules. For example, to explain rapid aggregation of NPs at high ionic strengths (typically $>10^{-2}$ M), their aggregation kinetics model assumes that the magnitude of the repulsive surface charge density of the diffuse layer decreases with the ionic strength. In fact, this is not the case for TiO_2 NPs immersed in an 1:1 aqueous solution (like NaCl or KCl) because the magnitude of their surface charge density (at the surface of the mineral) increases with salinity and therefore the magnitude of the surface charge density of the diffuse layer also increases with salinity to cancel it [8, 9]. Zhang et al. [42] developed an aggregation kinetics model based on the Maxwell approach. These authors assume that NP aggregation is controlled mainly by their random kinetic motion because of their nanometric size. They consider that aggregation could occur exclusively among the fraction of NPs with the minimum kinetic energy that exceeds the interaction energy barrier. In their model, the dispersed NPs are assumed to be Brownian particles in dilute systems. That may be true for elementary NPs with a low surface charge density, but NPs are often present in the form of aggregates in environmental media and the metal oxide NP like TiO_2 NP has a large energy barrier due to its high surface charge density [8, 9, 18]. Moreover, this aggregation kinetics model [42], as opposed to aggregation

kinetics models based on the DLVO theory, needs an additional fitting parameter to account for the hydrodynamic damping effect.

According to the DLVO theory and for perikinetic aggregation (by diffusion), the stability ratio is defined by the following equation [43]:

$$W = \frac{k_f}{k_s} = \frac{\int_{\min(u_a)}^{\infty} \beta(u_a) \frac{e^{V_{\mathrm{TOT}}(u_a)/k_b T}}{(u_a+2)^2} \mathrm{d}u_a}{\int_{\min(u_a)}^{\infty} \beta(u_a) \frac{e^{V_{\mathrm{VDW}}(u_a)/k_b T}}{(u_a+2)^2} \mathrm{d}u_a}, \quad (1)$$

where $\beta(u_a)$ is the correction factor for the hydrodynamic resistance between two approaching particles having radii a_1 (m) and a_2, $u_a = 2d/(a_1 + a_2)$, d is the surface-to-surface separation distance between the two particles (m), k_b is the Boltzmann constant (1.381×10^{-23} J K^{-1}), and T is the absolute temperature (K). The parameters V_{TOT} and V_{VDW} (in J) represent total and van der Waals interaction energies between the two particles, respectively. V_{TOT} is the sum of the attractive van der Waals interaction energy and the (generally) repulsive electrical double layer interaction energy, V_{EDL}. The sign and the strength of this double layer interaction energy are given by the surface electrical potential, commonly assumed to be the zeta potential (ζ) [19, 44]. The latter is therefore a key parameter for the estimation of NP aggregation kinetics and must be accurately calculated. This is the reason why, in section 3, the zeta potential is calculated by an electrostatic surface complexation model. The correction factor for hydrodynamic resistance is described by the following approximation [43]:

$$\beta(u_a) = \frac{6u_a^{\,2} + 13u_a + 2}{6u_a^{\,2} + 4u_a}. \quad (2)$$

According to the DLVO theory, Eq. (1) shows that the stability ratio of electrically charged and suspended particles is strongly controlled by interaction energies due to

VDW and EDL forces. Two different approaches can be used to estimate the interaction energies between two spherical particles from interaction energies per unit area between two infinite flat plates: the Derjaguin approximation (DA) and the surface element integration (SEI).

2.2. Interaction energies

2.2.1. Interaction energies between two infinite flat plates

The non-retarded van der Waals interaction energy per unit area (E_{VDW} ; J m^{-2}) between two infinite flat plates separated by a distance *h* is calculated according to the Hamaker approach [45] by:

$$E_{\mathrm{VDW}}(h) = -\frac{A_{\mathrm{H}}}{12\pi h^2}, \tag{3}$$

where A_{H} is the Hamaker constant (J) which includes the dielectric information for the particles and the surrounding medium. The attractive London-van der Waals force arises from the bulk material properties of the particles and is caused by dipolar fluctuation of the atoms. The strength of this force is independent of the chemical composition of water surrounding the particles, and it decreases very rapidly with the surface-surface separation distance [27].

There is, as yet, no universal theory describing double layer interaction energy when two particles collide because, in that case, there is an overlapping of the diffuse layers and the double layer is not in thermodynamic equilibrium [32, 33, 36]. Three different approaches can be used to analytically estimate EDL interaction energy per unit area: constant charge approximation (CCA) [46], constant potential approximation (CPA) [40] and linear superposition approximation (LSA) [47].

CCA considers that the surface charge density is, therefore, constant, as is the total number of counter-ions between the surfaces as the particles draw closer [46, 48]. The counter-ions concentration and the repulsive double layer pressure increase accordingly. CPA, on the other hand, assumes that the concentration of counter-ions between the two surfaces remains approximately constant and the surface charge density diminishes as the surfaces come together [40, 48]. Therefore, repulsive double layer interaction energies predicted by CCA are higher than those predicted by CPA. CCA and CPA are based on the linear Poisson-Boltzmann equation. These two methods consider a Debye-Hückel ionic atmosphere, i.e. that the electrical potential in the diffuse layer follows a Debye-Hückel distribution. Consequently, the analytical equations used by these two models (to estimate the double layer interaction energy per unit area) are accurate only for low surface electrical potentials (magnitude $< k_b T / ze$, where e is the elementary charge of 1.602×10^{-19} C and z is the valence of a binary symmetric electrolyte) [19, 44]. Furthermore, these two approximations may be regarded as extremes, with the "true" situation lying somewhere in between [2, 37, 49].

LSA is a useful compromise between CCA and CPA [2, 16, 47] that gives intermediate values for the double layer interaction energy per unit area [47, 49]. This theory is based on the calculation of the electrical potentials of isolated spheres, which can be done numerically. This means that LSA can be used for higher surface electrical potentials than CCA and CPA. This also means that LSA is particularly relevant when particles are far apart, i.e. in cases where $\kappa h >> 1$ [50], κ being the inverse of the Debye length, which corresponds to approximately half the total thickness of the diffuse layer of isolated particles [44]. According to LSA, the double layer interaction energy per unit area can be written as [51]:

$$E_{\mathrm{EDL}}(h) = 32\varepsilon_0\varepsilon_r\kappa\left(\frac{k_bT}{ze}\right)^2 y_1 y_2 e^{-\kappa h}, \quad (4)$$

with

$$y_{1,2} = \tanh\left(\frac{ze\psi_{d1,2}}{4k_bT}\right), \quad (5)$$

where ε_0 is the dielectric permittivity of vacuum (8.85×10^{-12} F m^{-1}), ε_r is the relative dielectric permittivity of water ($\varepsilon_r \cong 78.3$ for bulk water at a pressure = 1 bar and a temperature T = 298 K), and ψ_d is the electrostatic potential at the head-end of the diffuse layer (in V), which corresponds to the outer Helmholtz plane (OHP). This electrostatic potential is called the surface electrical potential, commonly assumed to be equal to the zeta potential (ζ) [19, 44].

The inverse of the Debye length, κ, is calculated by :

$$\kappa = \sqrt{\frac{2000e^2 N_A I}{\varepsilon_0\varepsilon_r k_b T}}, \quad (6)$$

$$I = 0.5\sum_{i=1}^{N} z_i^2 c_i^b, \quad (7)$$

where N_A is the Avogadro number (6.022×10^{23} mol^{-1}), I is the ionic strength of the solution (mol dm^{-3}), N is the number of types of ions in the bulk electrolyte (superscript "b") of valence z_i, and concentration c_i (mol dm^{-3}).

2.2.2. Derjaguin approximation and surface element integration

The Derjaquin approximation (DA) enables us to calculate the interaction energy, V, between two spherical surfaces from the interaction energy per unit area between two plane surfaces, E, according to [28]:

$$V_{\mathrm{DA}}(d) \approx \int_A E(h)\,\mathrm{d}A \approx \frac{2\pi a_1 a_2}{a_1 + a_2} \int_d^\infty E(h)\,\mathrm{d}h \ , \tag{8}$$

where *d* is the distance of closest approach between the two curved surfaces and *A* is the area of the facing surfaces. Equations for the calculation of the interaction energies are written in Appendix A.

The main assumption in the Derjaguin approximation is that the range of the interaction energy is much shorter than the radii of curvature of the particles. The function outside of the integral in Eq. (8) represents curvature effects that are valid only near the distance of closest approach, *d*. This means that DA is accurate if the distance between the two surfaces is much smaller than the shortest radius of the two particles, i.e. when $d << a_{\min}$ [52]. This also implies that DA is accurate for thin double layers relative to the smallest radius, i.e. when $\kappa a_{\min} > 10$ [51]. Furthermore, Derjaguin's technique considers that a surface element interacts with another element directly facing it with an intensity *E*(*h*). This assumption becomes progressively inaccurate as the separation distance between particles increases. DA overestimates the interaction energy between two particles when the condition $d << a_{\min}$ is not satisfied [51-53]. To avoid the main assumptions of DA, we use a specific computing method, surface element integration (SEI), which discretizes the area over which the two surfaces interact.

The surface element integration method calculates the total interaction energy between two particles by numerically integrating the interaction energy per unit area between opposing differential planar elements over the entire surfaces. For two spherical particles and according to the SEI method, the interaction energy can be written as:

$$V_{\mathrm{SEI}}(d) = \int_{S_1} \mathrm{d}V = \int_{A_1} \mathbf{n_2} \cdot \mathbf{k_2} \frac{\mathbf{n_1} \cdot \mathbf{k_1}}{|\mathbf{n_1} \cdot \mathbf{k_1}|} E(h)\,\mathrm{d}A_1 \ . \tag{9}$$

In Eq. (9), the centers of particles 1 and 2 are origins of two body-fixed coordinate systems, with their *z* axes directly facing each other (Fig. 1). The *xy* planes of these coordinate systems are parallel to each other (see Bhattacharjee et al. [51] for more details relative to SEI). The parameter S_1 in Eq. (9) is the surface of particle 1, A_1 is the projected area of particle 1 on the *xy* plane, vectors $\mathbf{n_1}$ and $\mathbf{n_2}$ are the outward unit normal to the surfaces of the two particles, and vectors $\mathbf{k_1}$ and $\mathbf{k_2}$ are the unit vectors directed towards the positive *z* axes of each body-fixed coordinate system. The scalar products $\mathbf{n_1} \cdot \mathbf{k_1}$ and $\mathbf{n_2} \cdot \mathbf{k_2}$ can have both positive and negative values. Equations for the calculation of the interaction energies are written in Appendix A.

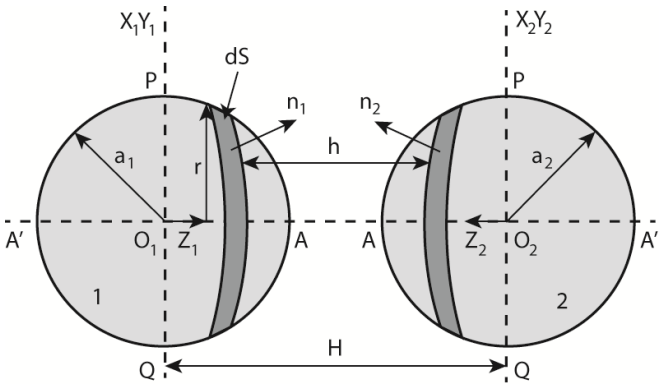

Fig. 1. Two interacting spherical particles with radii a_1 and a_2. The centers of the spheres are origins of two body-fixed coordinate systems, with their *z* axes directly facing each other. The *xy* planes of these coordinate systems are parallel to each other (from Bhattacharjee et al. [51]).

According to Bhattacharjee et al. [51], SEI, on the contrary to DA, doesn't grossly overestimate the repulsive double layer interaction energy between particles (with the same radius *a*) when $\kappa a < 10$. This can be the case for NPs immersed in a dilute aqueous solution. Furthermore, Eqs. (8) and (9) are based on the assumption of pairwise interaction between two facing surface elements. The error involved in this assumption

will be small only when the interaction energy is very short-ranged. These two equations assume that the interaction force per unit area acts normal to the particle surface, which is rigorous only for a constant surface potential [51].

2.3. Zeta potential

Snoswell et al. [22] used Henry equation [54] to convert electrophoretic mobility measurements of TiO_2 nanoparticles into apparent zeta potentials. However, this equation only considers the retardation effect associated with the size of the particle. The conversion of electrophoretic mobility measurements of metal oxide NPs is very difficult because these particles have an electrical double layer which affects the applied electrical field around the particle [18] (Fig. 2). Surface conductivity is associated with the electromigration of electrical charges in the double layer around the particle and is inversely proportional to the size of the particle [18-21]. It creates a retardation force that decreases the magnitude of the electrophoretic mobility of the particle if surface conductivity is similar to or higher than the bulk electrical conductivity [18, 55]. Therefore, apparent zeta potentials (not corrected of surface conductivity) can be significantly lower than true or intrinsic zeta potentials. Furthermore, Snoswell et al. [22] made not a complete set of electrophoretic mobility measurements. These authors therefore used an empirical interpolation formula to obtain zeta potentials at any pH and ionic strength.

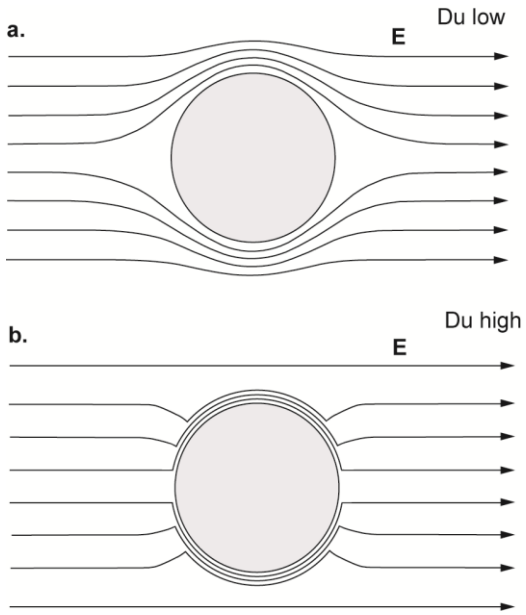

Fig. 2. Effect of the electrical double layer around the particle on the applied electrical field. Non-conducting particles (**a.**) and conducting particles (**b.**) (from Lyklema and Minor [55]). Du is the Dukhin number, which is defined as half the ratio of surface electrical conductivity to bulk electrical conductivity.

As shown by Eq. (5), the electrostatic potential at the OHP, ψ_d, is a key physicochemical parameter for describing the repulsive double layer interaction energy between TiO_2 NPs. In the double layer theory, the electrostatic potential at the OHP is usually assumed to be equal to the zeta potential (ζ) which can be inferred from electrophoretic mobility measurements, for example [19, 44]. Under the applied electrical field, hydrated counter-ions in the diffuse layer drag water molecules and therefore create a solvent flow at the surface of the particles. This solvent flow is therefore assumed to be zero at the onset of the diffuse layer which coincides with the shear plane where the zeta potential is located [19, 44].

As opposed to what was done in previous studies [10, 22], the electrostatic potential at the OHP, ψ_d, is calculated directly by the extended Stern model of Leroy et al. [18]

(Fig. 3) and is therefore not derived directly from the electrophoretic mobility measurements. The parameters of this electrostatic surface complexation model were calibrated using ab-initio calculations (done with the Density Functional Theory, DFT), crystallographic studies, electrophoretic mobility and potentiometric titration measurements of pure TiO_2 NPs (Degussa P25) [8, 18]. Ridley et al. [25] emphasized that the size and shape of TiO_2 nanoparticles have little influence on their measured surface charge densities. In our approach, the electrochemical properties of the TiO_2 nanoparticles used by Snoswell et al. [22] are therefore assumed to be very close to the electrochemical properties of the TiO_2 nanoparticles used by Leroy et al. [18]. This justifies the use of the extended Stern model of Leroy et al. [18].

To confirm this assumption, we also use the approach of Leroy et al. [18] to convert electrophoretic mobilities of Snoswell et al. [22] into zeta potentials using Henry's electrokinetic transport model [56]. Therefore, experimental zeta potentials can be compared to zeta potentials predicted by our electrostatic surface complexation model. Because the two materials have slightly different pH_{IEP} (IEP is the isoelectric point, a pH_{IEP} equal to 6.3 was reported in the work of Leroy et al. [18] and a pH_{IEP} equal to 6.1 was reported in the work of Snoswell et al. [22]), the value of the equilibrium constant (K) for the sorption of protons at the $>Ti_2O^{-0.57}$ surface sites is modified (the initial value of $\log K = 7.55$ [18] is replaced by $\log K = 7.1$).

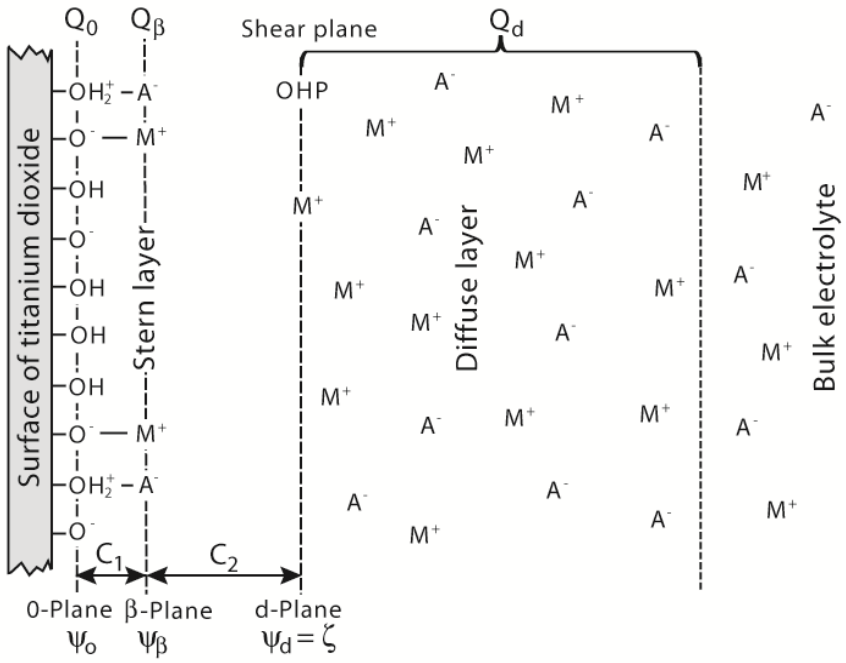

Fig. 3. The simplified sketch of the extended Stern model (ESM) of Leroy et al. [18]. M^+ are metal cations (e.g., Na^+ or K^+) and A^- are anions (e.g., Cl^-). OHP is the outer Helmholtz plane, which corresponds here to the shear plane where the zeta potential (ζ) is defined. Q is the surface charge density of the three different layers (mineral surface, Q_0, Stern, Q_β, and diffuse layer, Q_d). C is the capacitance between the "0-plane" and the "β-plane" (C_1), and between the "β-plane" and the "d-plane" (C_2).

According to Henry [56], the surface conductivity and the internal conductivity of an electrically charged particle alter the shape of the potential distribution of the applied field in the liquid, modify the fluid motion within the electrical double layer, and therefore change the fluid stresses exerted on the particle. For spherical particles, Henry ([56]) proposed:

$$\zeta = \frac{3\eta}{2\varepsilon_0\varepsilon_r}\frac{1}{\{1+2\lambda[f(\kappa a)-1]\}}\mu, \tag{10}$$

$$\lambda = \frac{1 - K' - 2\,\mathrm{Du}}{2 + K' + 2\,\mathrm{Du}}, \tag{11}$$

$$K' = \frac{\sigma_p}{\sigma_b}, \tag{12}$$

$$\mathrm{Du} = \frac{\sigma_s}{2\sigma_b} = \frac{\Sigma_s}{a\sigma_b}, \tag{13}$$

where η is the dynamic viscosity of water (in Pa s; $\eta = 0.895\times10^{-3}$ Pa s at $T = 298$ K), λ is the dipolar coefficient of the particle, and $f(\kappa a)$ is a correction factor taking into account the retardation effect due to the size of the particle ([57], comprised between 1, Hückel theory [58], and 1.5, Smoluchowski theory [59]). σ is the electrical conductivity (in S m^{-1}), Σ is the specific surface electrical conductivity of the electrical double layer (in S), subscripts "*p*", "*s*", "*b*" correspond, respectively, to the particle's "interior" (aggregates of elementary NPs), the particle's surface and the surrounding medium (the bulk aqueous electrolyte). The specific surface conductivity expresses the excess of electrical conductivity at the solid's surface compared to that of the bulk aqueous electrolyte [60-63]. Du corresponds to the Dukhin number (see Dukhin and Shilov [64] for more details concerning this parameter). Equations used for the calculation of the parameters $f(\kappa a)$, σ_p, σ_b, and Σ_s are written in Appendix B.

Electrophoretic mobilities are converted into true zeta potentials using Eqs. (10)-(13) and (B1)-(B8), in order to compare them with the ψ_d values calculated by our ESM. The fitting parameters for the conversion procedure are the radius of the aggregate (which varies with pH and salinity), *a*, the radius of elementary nanoparticles (which does not vary with pH and salinity), a_e and the intra-aggregate porosity ϕ, (the surface mobility of adsorbed counter-ions at the Stern layer is considered to be equal to their

mobility in bulk electrolyte). Specific surface conductivities of the Stern and diffuse layers are estimated directly by our electrostatic surface complexation model.

3. Comparison with experimental data

We test our approach combining an electrostatic surface complexation and an aggregation kinetics model, to see if it could predict measured stability ratios of pure synthetic TiO_2 NPs (immersed in a KCl solution at different pH values (6.3, 6.7 and 8.4) [22]). The parameters required are the minimum separation distance between NPs, $d_{\min}$, the (non retarded) Hamaker constant, A_H, and the effective interaction radius, a_i. The electrostatic potential ψ_d, which is directly calculated by the ESM, is compared to the zeta potential inferred from the electrophoretic mobility measurements of Snoswell et al. [22] using the approach of Leroy et al. [18]. Stability ratios predicted by LSA-DA, and LSA-SEI are compared to the measured stability ratios of Snoswell et al. [22].

3.1. Zeta potential

The TiO_2 NPs zeta potentials reported by Snoswell et al. [22] and calculated with the approach of Leroy et al. [18] are shown in Figs. 4a and 4b, respectively. Snoswell et al. [22] used Henry's equation without surface conductivity correction (Eq. (10) with λ = 0.5) to estimate the zeta potentials from the measured electrophoretic mobilities. These "observed" zeta potentials can be compared to the zeta potentials directly predicted by the ESM (assuming $\psi_d = \zeta$). ESM calculations are done with PHREEQC [65].

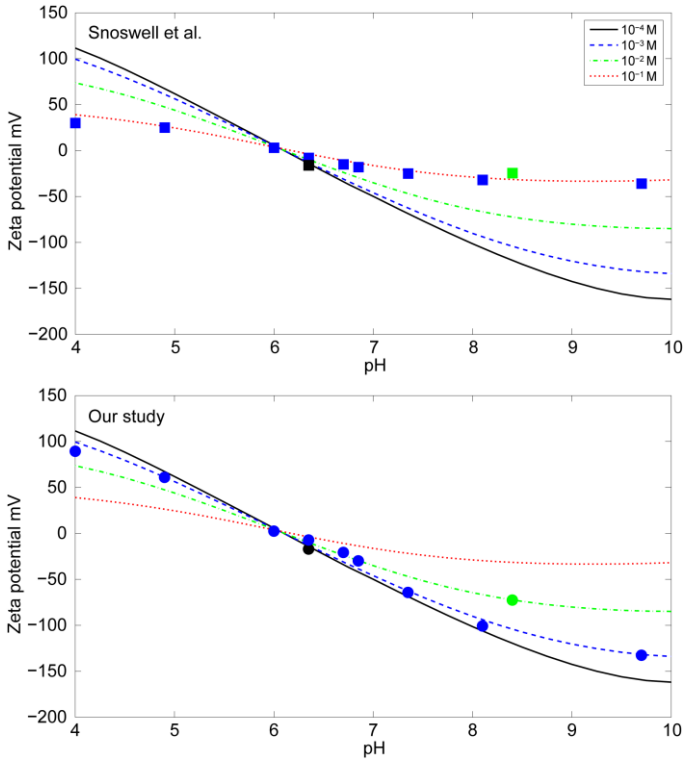

Fig. 4. "Observed" zeta potentials of pure TiO_2 NPs versus pH at 10^{-4}, 10^{-3}, and 10^{-2} M KCl from Snoswell et al. [22] (**a**; squares) and calculated using the approach of Leroy et al. [18] (**b**; circles). The curves are the ESM predictions assuming $\psi_d = \zeta$ [18].

Because of the strong influence of surface conductivity on the electrophoretic mobilities of TiO_2 NPs, zeta potentials estimated by Snowswell et al. [22] are significantly underestimated compared to the zeta potentials predicted by the surface complexation model (ESM), especially at low ionic strengths and pH values distant from the pH_{IEP} ($pH_{IEP} = 6.1$) (Fig. 4a). pH_{IEP} is the pH of isoelectric point. It is the pH value where the zeta potential is equal to zero.

This is not the case if the approach of Leroy et al. [18] is used to convert electrophoretic mobilities into zeta potentials taking into account surface conductivity (Fig. 4b). Underestimation of the true zeta potentials by Snoswell et al. [22] can be explained by the very high Dukhin number of the elementary NPs and their aggregated forms. This

high value of the surface conductivity of NPs compared to that of colloids and larger particles is readily justified because this phenomenon is inversely proportional to particle size [55] (Eqs. (13) and (B4)) (Fig. 5).

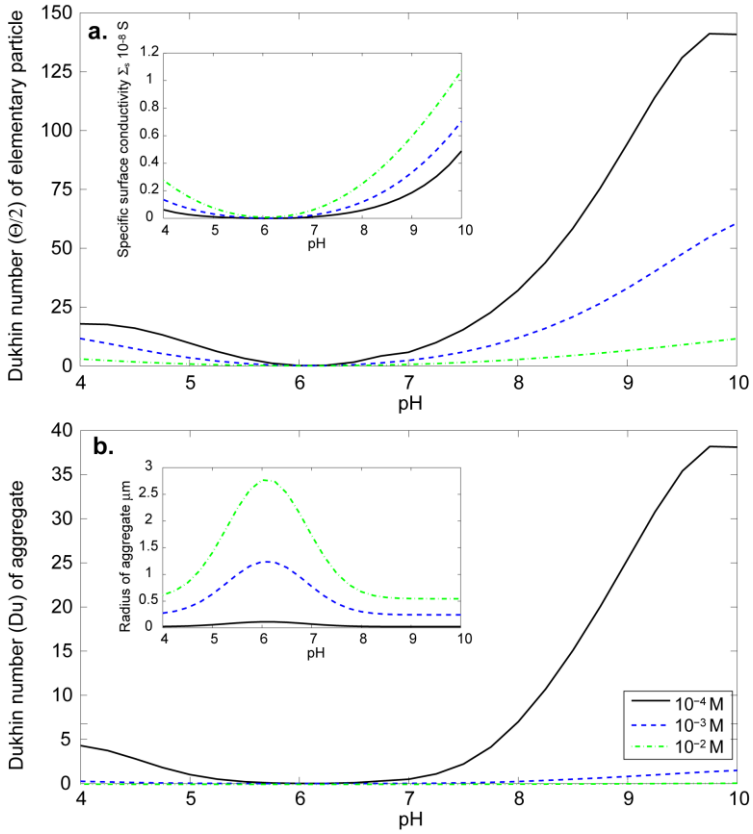

Fig. 5. The predicted Dukhin numbers of (**a**) an elementary NP and (**b**) an aggregate versus pH at 10^{-4}, 10^{-3}, and 10^{-2} M KCl. The mean radius of elementary NPs is equal to 6 nm ([22]), and the radius of the aggregate is optimized by decreasing the cost function $R^2 = \sum_{i=1}^{L}\left[\zeta_{\text{obs}}(i) - \psi_d(i)\right]^2$ using the Simplex algorithm [66] (where L is the number of experimental values). The intra-aggregate porosity is equal to 10 %.

The Dukhin number increases as the ionic strength of the aqueous solution decreases because the ratio of surface to bulk electrical conductivity increases with the dilution of the aqueous electrolyte (Eq. (13)). Furthermore, when pH moves away from pH_{IEP}, the

Dukhin number increases because the specific surface conductivity increases (Fig. 4a). This can be explained by the increasing concentration of counter-ions in the Stern and diffuse layers (Eq. (B7); Γ_i^{St} and ψ_d increase when pH moves away from pH_{IEP}).

Snoswell et al. [22] significantly underestimated the true zeta potentials and therefore the repulsive double layer energy between particles. This implies that, in their aggregation kinetics modeling, they adjusted the Hamaker constant A_H with an unrealistic value ($A_H = 2\times10^{-20}$ J for the TiO_2-H_2O-TiO_2 interface, see also section 1). Their Hamaker constant is significantly lower than typical estimates. For instance, Larson et al. [23] found $A_H = 6\pm2\times10^{-20}$ J for the TiO_2-H_2O-TiO_2 interface using the DLVO theory and successfully predicted the interaction force between a rutile TiO_2 colloid (diameter of approximately 9 μm) and a single macroscopic rutile crystal in an aqueous solution. This force was measured at the isoelectric point of the TiO_2/water interface (where no double layer interaction should occur) by Atomic Force Microscopy (AFM). To date and to our knowledge, no study has shown that there is a correlation between the Hamaker constant and particle size for metal oxide NPs. The calculations done by Larson et al. [23] seriously question the value of the Hamaker constant deduced by Snoswell et al. [22]. The A_H value found by Snoswell et al. [22] is also significantly lower than the Hamaker constant estimated using spectroscopy data ($A_H = 7\pm1\times10^{-20}$ J [23]) and the full Lifshitz theory ($A_H = 7.7\pm1.7\times10^{-20}$ J [24]; $A_H = 5.5\pm0.5\times10^{-20}$ J [67]).

3.2. Aggregation kinetics

The evolution of the hydrodynamic radius of the aggregate with time (for a given chemical composition of the aqueous solution) can be expressed by the stability ratio *W*.

This was determined experimentally by Snoswell et al. [22], who measured the ratio of the fast kinetic constant, k_f, to the slow kinetic constant, k_s. The two kinetic constants are proportional to the slope of the hydrodynamic radius a_h versus time *t* as $t \to 0$ s for each electrolyte concentration. Measured stability ratios enable the estimation of the critical coagulation concentration (CCC) [16]. The critical coagulation concentration is one of the most significant properties of NPs in suspension. It is defined as the minimum electrolyte concentration needed to induce fast aggregation of NPs, i.e. at CCC, the stability ratio is 1 ($\log(W) = 0$).

3.2.1. A priori parameters

Our aggregation kinetics model involves four parameters: electrostatic potential at the OHP, ψ_d, minimum separation distance between NPs, $d_{\min}$, (non-retarded) Hamaker constant, A_{H}, and the particle's effective interaction radius, a_i. The electrostatic potential ψ_d is calculated by the ESM, whereas $d_{\min}$, A_{H} and a_i need to be optimized.

As suggested by Frens and Overbeek [33], the minimum separation distance between NPs must be superior to twice the distance δ between the center of the surface atoms of the particle and the outer Helmholtz plane, i.e. $d_{\min} > 2\delta$. For $d \le 2\delta$, counter-ions would be squeezed between the particles' surfaces. Such a violation of the electroneutrality of the double layer systems would give rise to a strong repulsion, which could not be overcome by the relatively weak van der Waals attraction between the particles. δ can be estimated using the following equation [68]:

$$\delta = \frac{\varepsilon_0 \varepsilon_{r1}}{C_1} + \frac{\varepsilon_0 \varepsilon_{r2}}{C_2}, \tag{14}$$

where C_1 and C_2 are capacitances (in F m^{-2}) of the two molecular capacitors of the ESM (Fig. 3). The first molecular capacitor corresponds to the interfacial region located between the "0-plane" and the "β-plane" with a relative dielectric permittivity ε_{r1} (in F m^{-1}) while the second molecular capacitor corresponds to the region located between the "β-plane" and the "d-plane" with a relative dielectric permittivity ε_{r2}. In accordance with Bourikas et al. [9], and Hiemstra and Van Riemsdijk [68], we choose $\varepsilon_{r1} = 39.15$ and $\varepsilon_{r2} = 78.3$. The value of ε_{r1} is half the value of ε_{r2} because of the presence of a strong electrical field between the "0-plane" and the "β-plane". The capacitance values are $C_1 = 2.5$ F m^{-2} and $C_2 = 1$ F m^{-2} [18]. Using Eq. (14) and the C and ε_r values given above, we obtain $\delta = 0.83$ nm. This means that $d_{\min} > 1.66$ nm.

The optimized values of the three parameters are determined using a MatLab routine and the Simplex algorithm [66] for which starting values are $d_{\min} = 1.66$ nm, $A_H = 6 \times 10^{-20}$ J [23] and a_i = 150 nm. The a priori value of a_i is given according to dynamic light scattering measurements of TiO_2 primary particles in dilute water and for a pH value (not given by the authors) close to pH_{IEP} (pH_{IEP} = 6.1) [22].

3.2.2. Stability ratios

The Hamaker approach [45] and LSA [47] are used to calculate the interaction energies per unit area between two infinite flat plates due to van der Waals and double layer interactions (Eqs. (3) and (4), respectively). Interaction energies between two spherical particles with the same radius a_i were calculated accordingly using DA ([28]; Eqs. (A10) and (A11)) and SEI ([51]; Eqs. (A12)-(A16)). Stability ratios were determined

with Eqs. (1) and (2). The algorithm of optimization minimizes a cost function R^2 defined in a least square sense:

$$R^2 = \sum_{i=1}^{M} \{\log[W_{\text{obs}}(i)] - \log[W_{\text{cal}}(i)]\}^2 , \quad (15)$$

where M is the number of experimental values.

In the optimization procedure, two cases are considered. In the first case, the effective interaction radius is constant with pH. In the second case, the effective interaction radius varies with pH. As already stated by Snoswell et al. [22] and Schwarzer and Peukert [69], we suggest that the aggregation behavior of TiO_2 NPs can be controlled by NPs or small clusters of NPs with an effective interaction radius that can be shorter (low electrolyte concentration) or longer (high electrolyte concentration) than the Debye length. This implies that TiO_2 NPs aggregation kinetics can be controlled by nanoparticles or small clusters of nanoparticles rather than aggregates [22, 69]. Schwarzer and Peukert [69] stated that, if the range of interaction (determined by at least two times the Debye length, κ^{-1}) is smaller than the size of the nanoparticle (this can be the case for an ionic strength greater than approximately 10^{-3} M where $\kappa^{-1} \cong 9.8$ nm), the interaction energy of aggregates is determined only by the two nanoparticles involved (Fig. 6). Furthermore, Schwarzer and Peukert [69] emphasized that, if the range of interaction is similar to or longer than the size of the nanoparticle (this can be the case for an ionic strength lower than approximately 10^{-3} M because the Debye length increases with the dilution of the aqueous solution, see Eq. (6)), the interaction energy depends not only on the nanoparticles in contact but also on neighboring particles and their distance to contact, i.e. the local structure of the aggregate. This implies that the effective interaction radius can vary with ionic strength. Because stability ratios were recorded by Snoswell et al. [22] at different pH values with different salinity ranges, we

assume, like Snoswell et al. [22], that the effective interaction radius can vary with pH rather than with ionic strength (in order to limit the number of adjusted radii).

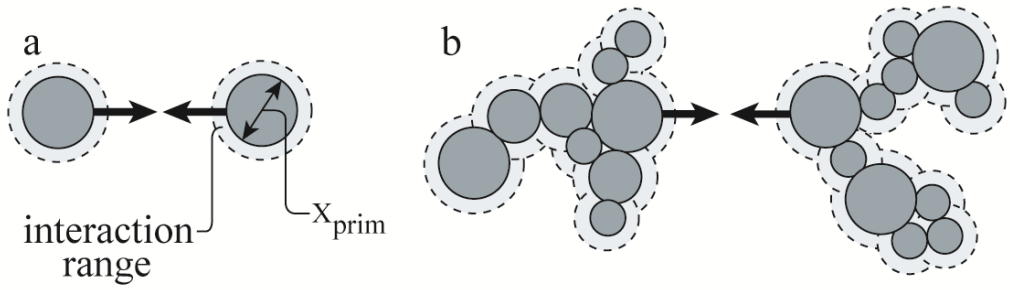

Fig. 6. The aggregation behavior of two nanoparticles (**a**) and of two aggregates (**b**) showing that stability is determined by the two nanoparticles involved if the range of interaction (defined by the thickness of the diffuse layer) is largely inferior to their size (from Schwarzer and Peukert [69]).

Stability ratios predicted using both approaches (DA and SEI) are in very good agreement with the experimental data of Snoswell et al. [22], except for the pH value very close to the pH_{IEP} (pH = 6.3) (Fig. 7). When the effective interaction radius is considered to vary with pH, our stability ratio predictions improve significantly, particularly at pH = 6.3 and for ionic strengths lower than approximately 10^{-3} M. According to Schwarzer and Peukert [69], at low ionic strengths, the local structure of the aggregate can control its aggregation behavior. Therefore, under these physicochemical conditions, a larger effective interaction radius is needed to reproduce the trend of the experimental data (according to the DLVO theory, predicted stability ratios increase with the radius of the particle [16]).

At pH = 6.3, a combination of LSA and DA gives better predictions of stability ratios than a combination of LSA and SEI. LSA is very good for large separation distances and less efficient for small separation distances while DA overestimates the interaction

energy for large separation distances but is efficient for small separation distances. Consequently, the LSA-DA combination is a good compromise that covers all of the separating distances between particles [47, 50]. The present approach can also accurately predict CCC, which increases with pH. This can be explained by the increasing magnitude of the surface electrical potential and repulsive double layer force when pH moves away from pH_{IEP} (Fig. 4).

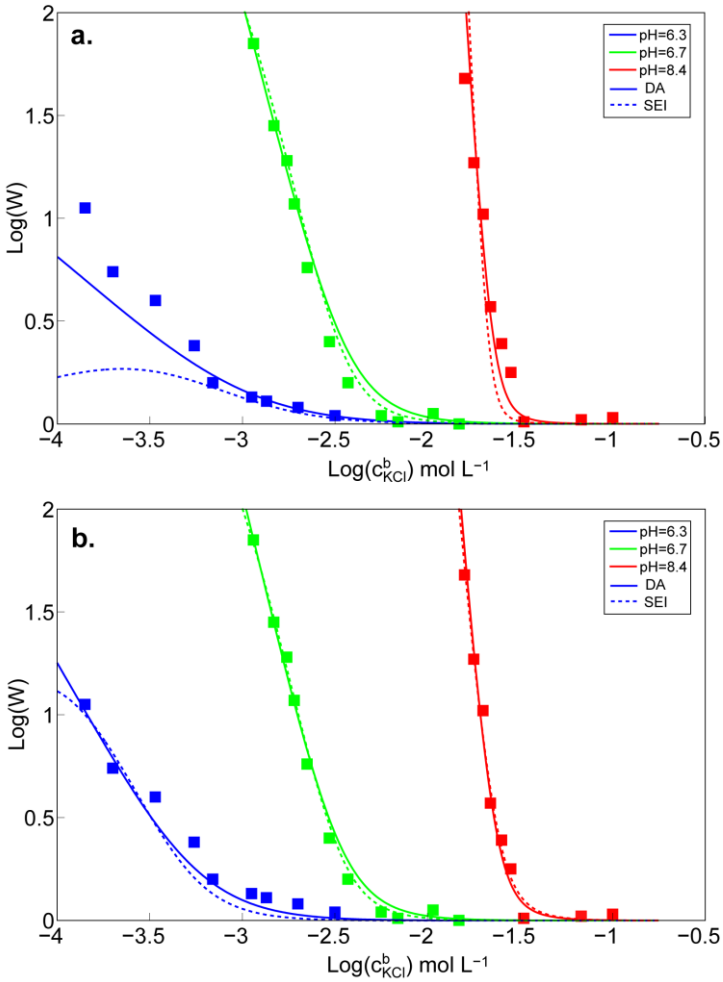

Fig. 7. Stability ratios versus salinity (KCl) (in log scale) at three different pH values (pH = 6.3, 6.7, and 8.4). Experimental data from Snoswell et al. [22] (squares) and model predictions with DA (solid lines) and SEI (dotted lines). Two cases are considered: the effective interaction radius is constant with pH (**a**) and the effective interaction radius varies with pH (**b**).

During slow aggregation, also called reaction limited clusters aggregation (RLCA) [16], there is a strong electrostatic barrier between particles, $\log(W) > 0$, and the aggregation rate depends strongly on the salt concentration (Fig. 7). In that case, not all collisions lead to sticking events, and individual particles have time to find a pathway into the core of a compact aggregate [16, 70] (mass fractal dimension *D* = 2.1-2.2 [70]). During fast aggregation, also called diffusion limited clusters aggregation (DLCA), the interaction energy between particles is purely attractive (due to van der Waals interactions), $\log(W) = 0$, and the aggregation rate no longer depends on the salt concentration (Fig. 7). In that case, diffusion of clusters controls the aggregation process [16], leading to larger and less compact aggregates (compared to RLCA; mass fractal dimension *D* = 1.7−1.8 [70]). In the intermediate phase between slow and fast aggregation, there is a gradual transition between RLCA and DLCA [16, 70].

The quality of the stability ratio predictions decreases when the pH of the solution is close to pH_{IEP} (at pH = 6.3) and when the salinity is close to the CCC. It is very difficult to reproduce the evolution of stability ratios when the pH of the aqueous solution is close to pH_{IEP} and in the transition phase between the slow and fast aggregation [10, 16, 70]. This is because, under these physicochemical conditions, repulsive double layer forces are relatively weak compared to attractive van der Waals forces and, therefore, TiO_2 NPs aggregation kinetics may be controlled by the collision of more than two isolated particles [40, 71].

3.2.3. Optimized parameters and interaction energy profiles

Values of adjusted parameters are given in Table 1 (constant effective interaction radius) and Table 2 (variable effective interaction radius). In all cases, the minimum separation distance is significantly greater than the a priori value (1.66 nm). This might be due to the uncertainty associated with the estimation of δ. Indeed, in Eq. (14), the dielectric permittivities ε_{r1}, ε_{r2}, and the capacitance C_2 are not precisely known [68]. The capacitance C_2 remains relatively unknown because the dielectric permittivity ε_{r2} and the location of the shear plane (where the zeta potential is located) are still uncertain [55] ($C_2 = \varepsilon_{r2}/(x_d - x_\beta)$ where x_β and x_d are the locations of the "β-plane" and the "d-plane", which corresponds to the shear plane, from the TiO_2's surface). A second reason for the large $d_{\min}$ value might be an overestimation of the electrostatic potential ψ_d by our ESM. The capacitance C_2 of our ESM is the parameter most subject to some uncertainty because, as cited above, the location of the shear plane remains relatively unknown. A lower capacitance C_2 value would lead to a lower magnitude of the electrostatic potential ψ_d. A third reason might be due to the DLVO theory, which overestimates interaction energies between NPs [22, 29, 37], in particular for small separation distances. Indeed, it has been observed that the DLVO theory overestimates interaction energies between TiO_2 particles for small separation distances [23]. For example, Larson et al. [23] found a good agreement between surface force measurements and predictions (with the DLVO theory) at a minimum separation distance of only 10 nm.

When the effective interaction radius is assumed to vary with pH, $d_{\min}$ decreases compared to the case when the effective interaction radius is assumed to be constant with pH (Table 2). Furthermore, when a_i varies with pH, our stability ratio predictions

are almost entirely independent of the value of d_{min} chosen (Table 2; the cost function R^2 increases slightly as the d_{min} value decreases). This implies that considering an effective interaction radius that varies with pH not only increases the accuracy of our stability ratio predictions, but it also decreases significantly the dependence of our stability ratio predictions on the value of d_{min}.

The optimized Hamaker constant and radius given by SEI are greater than those given by DA. This is because DA overestimates the van der Waals and double layer interaction energies of small particles (relative to the Debye length) compared to SEI [51]. Aside from this disagreement between DA and SEI in the estimation of the parameters, on the contrary to Snoswell et al. [22], the optimized Hamaker constants are similar to values found in the literature [23, 24, 67].

When the effective interaction radius is assumed to be constant with pH (Fig. 7a), its optimized values are close to the mean radius of the surface crystallites that constitute the aggregate (a_e is between 6 and 20 nm according to Snoswell et al. [22]; Table 1). This implies that TiO_2 NPs aggregation kinetics are controlled by surface crystallites or small clusters of surface crystallites rather than by aggregates, as reported by Schwarzer and Peukert [69]. When the effective interaction radius is assumed to vary with pH (Fig. 7b), its optimized values increase with the dilution of the aqueous solution (Table 2). These results agree with the statements of Schwarzer and Peukert [69] who emphasized that, if the range of interaction is similar to or longer than the size of the nanoparticle, the interaction energy will depend on the local structure of the aggregate.

Interaction energy profiles calculated using the two approaches (DA and SEI) for the three pH values and for a salinity of 10^{-2} M KCl, are shown in Fig. 8a. This salinity corresponds approximately to CCC at pH = 6.7 (Fig. 7). For low pH values (pH = 6.3,

6.7), the interaction energies between particles are only attractive because repulsive double layer forces are weak compared to van der Waals forces. At a higher ionic strength, $10^{-1.5}$ M KCl (which corresponds approximately to CCC at pH = 8.4), the repulsive energy barrier at pH = 8.4 disappears almost entirely (Fig. 8b).

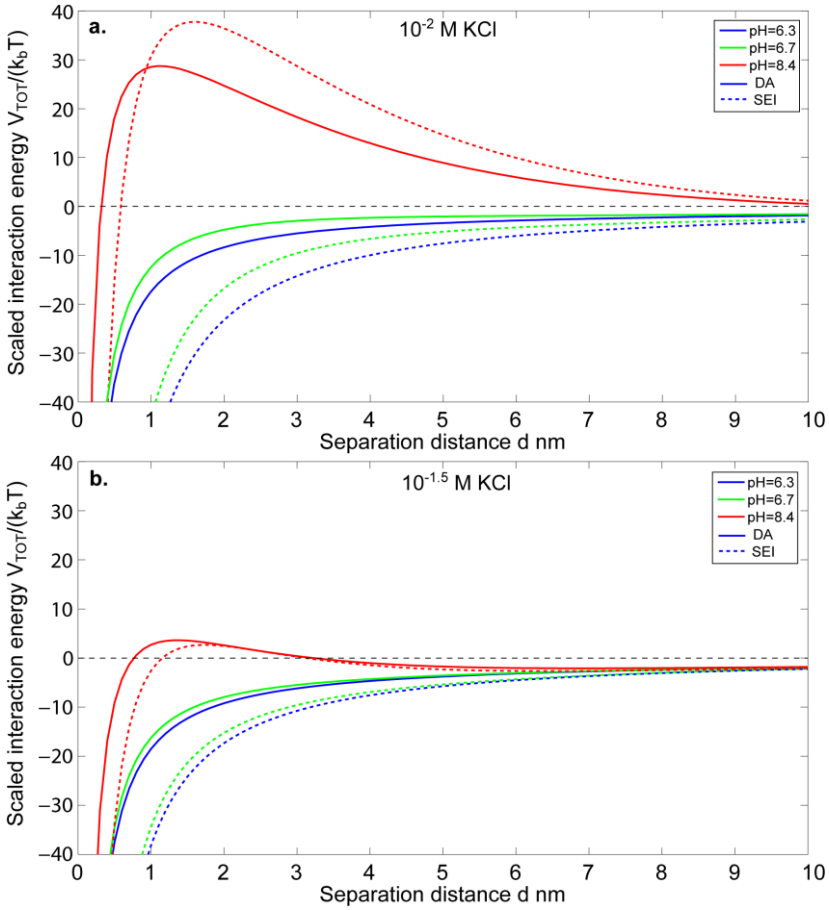

Fig. 8. Interaction energy profiles calculated by DA (solid lines) and SEI (dotted lines) at three different pH values (pH = 6.3, 6.7, and 8.4) and in the case of a constant effective interaction radius. **a.** Salinity of 10^{-2} M KCl. **b.** Salinity of $10^{-1.5}$ M KCl.

Our results show that the DA method is easily adjustable with three parameters (minimum separation distance, Hamaker constant, and effective interaction radius) while the SEI method is theoretically more suitable for NPs due to their nanometric size [51]. Moreover, considering an effective interaction radius that decreases with pH

increases significantly the accuracy of our stability ratio predictions. Our results do not agree with the effective interaction radii obtained by Snoswell et al. [22], whose optimized effective interaction radius increases with the pH of the aqueous solution (they found a_i values of 6, 12, and 20 nm at pH levels of 6.3, 6.7, and 8.4, respectively). In our approach, the introduction of true zeta potentials predicted by our extended Stern model reversed this trend because the retardation effect of surface conductivity is more pronounced when the ionic strength of the aqueous solution is low and the pH is distant from pH_{IEP}. We also find realistic values of Hamaker constants for the TiO_2-H_2O-TiO_2 interface. The approach proposed here appears, therefore, to be a real improvement, reaching a quantitative agreement with experimental results while using realistic parameterization.

4. Conclusions

We have developed a new approach based on DLVO theory to describe aggregation kinetics of titanium dioxide nanoparticles (NPs) in aqueous solutions. It has the advantage of using zeta potentials directly calculated by an extended Stern model (ESM) because the conversion of electrophoretic mobility measurements into zeta potentials is very difficult for metal oxide nanoparticles. This is due to their very high surface electrical conductivity associated with the electromigration of counter and co-ions in their electrical double layer and their very high surface-to-volume ratio. Linear superposition approximation (LSA) is combined with Derjaguin approximation (DA) or surface element integration (SEI) to calculate interaction energies of spherical particles. Zeta potentials calculated by our ESM and inferred from electrophoretic mobilities taking into account surface conductivity are found to be significantly higher in

amplitude than apparent zeta potentials (not corrected for surface conductivity). This is particularly the case at low ionic strengths (typically lower than 10^{-1} M) and pH values far away from pH_{IEP} (pH_{IEP} = 6.1) because, in these physicochemical conditions, surface conductivity is similar to or higher than the bulk electrical conductivity and, therefore, retardation effect due to surface conductivity is strong. The repulsive electrostatic force between NPs can be significantly underestimated if apparent zeta potentials are used instead of true zeta potentials.

Our two aggregation kinetics models (DA and SEI) are validated against measured stability ratios of pure synthetic TiO_2 NPs made at different pH values (pH = 6.3, 6.7, and 8.4) over a broad salinity range (between 10^{-4} and 10^{-1} M KCl). Optimized Hamaker constants for the TiO_2-H_2O-TiO_2 interface, comprised between 5.89 and 8.71×10^{-20} J, are in agreement with those reported in the literature. This confirms that DLVO theory is relevant to predict aggregation kinetics of TiO_2 NPs if the double layer interaction energy is estimated accurately.

The DA and SEI methods predict similar stability ratios, except at the lowest ionic strengths (lower to 10^{-3} M KCl) because DA overestimates significantly interaction energies when the interaction range can be similar to or longer than the size of nanoparticles. We also find that, in these physicochemical conditions, TiO_2 NPs aggregation kinetics are controlled by the local structure of the aggregate, whereas, at high ionic strengths, when the interaction range is shorter than the size of the nanoparticles, TiO_2 NPs aggregation kinetics are controlled by nanoparticles.

In the future, our approach can be used to predict the stability ratios of TiO_2 nanoparticles immersed in other aqueous electrolytes and to predict the stability ratios of other metal oxides nanoparticles. It can also used to better understand the contribution of each process (aggregation, deposition) that affects the mobility of NPs in

a flow-through column experiment. It can also contribute to quantitatively estimating the effect of the chemical composition of pore water (pH, ionic strength, the chemical nature of dissolved species) on the NPs reactive transport processes in porous media.

Acknowledgments

This paper is a part of the PhD thesis of Izzeddine Sameut Bouhaik, which is co-funded by the Carnot Institute –BRGM and the Region Centre. We would like to thank the editor and the anonymous reviewers for their efforts and constructive comments that contributed to improving our manuscript.

Appendix A

According to Derjaguin approximation, interaction energy V between two spherical particles can be expressed as a function of the interaction energy per unit area between two infinite flat plates E by:

$$V_{\mathrm{DA}}(d) \approx \int_d^{\infty} 2\pi r E(h)\,\mathrm{d}r, \tag{A1}$$

where d is the separation distance between the two spherical particles of radii a_1 and a_2 (see Fig. 1). The distance between two elements of surface, h, can be written by:

$$h = H \pm z_1 \pm z_2, \tag{A2}$$

where H is the distance between the centers of the two spherical particles of coordinates z_1 and z_2. Eq. (A2) can be written again by:

$$h = H \pm a_1\left(\sqrt{1 - r^2/a_1^2}\right) \pm a_2\left(\sqrt{1 - r^2/a_2^2}\right). \tag{A3}$$

Eq. (A3) can be simplified if the two closest surfaces (PAQ-PAQ) are only taken into account. This leads to:

$$h = H - a_1\left(\sqrt{1 - r^2/a_1^2}\right) - a_2\left(\sqrt{1 - r^2/a_2^2}\right). \tag{A4}$$

Derivative of Eq. (A4) gives:

$$\mathrm{d}h = \left\{ \frac{1}{a_1\left[\sqrt{\left(1 - r^2/a_1^2\right)}\right]} + \frac{1}{a_2\left[\sqrt{\left(1 - r^2/a_2^2\right)}\right]} \right\} r\,\mathrm{d}r. \tag{A5}$$

In the DA approach, radii are significantly larger than interaction distance. This implies:

$$\min(a_1, a_2) >> r \ . \tag{A6}$$

Therefore, by considering approximation (A6) in Eq. (A5), it follows:

$$\mathrm{d}h \approx \left(\frac{1}{a_1} + \frac{1}{a_2} \right) r\,\mathrm{d}r, \tag{A7}$$

$$r\,\mathrm{d}r \approx \left(\frac{a_1 a_2}{a_1 + a_2}\right)\mathrm{d}h\,. \tag{A8}$$

Finally, by combining Eqs. (A1) and (A8), the final DA equation is obtained:

$$V_{\mathrm{DA}}(d) \approx \frac{2\pi a_1 a_2}{a_1 + a_2}\int_d^{\infty} E(h)\,\mathrm{d}h\,. \tag{A9}$$

By combining Eqs. (3) and (A9), the attractive van der Waals interaction energy between two spherical particles can be calculated by [28]:

$$V_{\mathrm{VDW}}^{\mathrm{DA}} = -\frac{A_{\mathrm{H}} a_1 a_2}{6d\left(a_1 + a_2\right)}\,. \tag{A10}$$

The repulsive interaction energy due to the overlapping of the diffuse layers of the two spherical particles is estimated by combining Eqs. (4) and (A9):

$$V_{\mathrm{EDL}}^{\mathrm{DA}} = 64\pi\varepsilon_0\varepsilon_r y_1 y_2 \frac{a_1 a_2}{a_1 + a_2}\left(\frac{kT}{ze}\right)^2 e^{-\kappa d}\,. \tag{A11}$$

In the case of the surface element integration method, we can separate the surface of each particle (S_1 and S_2) into two hemispherical surfaces (PAQ and PA'Q) (Fig. 1). Four interaction energy terms are needed to calculate the total interaction energy between the two surfaces (S_1 and S_2). The signs of these terms depend on the different combinations of the signs of $\mathbf{n_1}\cdot\mathbf{k_1}$ and $\mathbf{n_2}\cdot\mathbf{k_2}$. The total interaction energy is the sum of all four interaction energy terms. The total interaction energy between two spherical particles, V_{SEI}, can be calculated by [51]:

$$V_{\mathrm{SEI}} = V_1 - V_2 - V_3 + V_4\,, \tag{A12}$$

where V_i (i =1, 2, 3, 4) is the surface-surface interaction energy. It can be written as:

$$V_1 = 2\pi \int_0^{a_1} \left(\sqrt{1-r^2/a_2^2}\right) E\left(d + a_1 + a_2 - a_1\sqrt{1-r^2/a_1^2} - a_2\sqrt{1-r^2/a_2^2}\right) r \, \mathrm{d}r \,, \tag{A13}$$

$$V_2 = 2\pi \int_0^{a_1} \left(\sqrt{1-r^2/a_2^2}\right) E\left(d + a_1 + a_2 + a_1\sqrt{1-r^2/a_1^2} - a_2\sqrt{1-r^2/a_2^2}\right) r \, \mathrm{d}r \,, \tag{A14}$$

$$V_3 = 2\pi \int_0^{a_1} \left(\sqrt{1-r^2/a_2^2}\right) E\left(d + a_1 + a_2 - a_1\sqrt{1-r^2/a_1^2} + a_2\sqrt{1-r^2/a_2^2}\right) r \, \mathrm{d}r \,, \tag{A15}$$

$$V_4 = 2\pi \int_0^{a_1} \left(\sqrt{1-r^2/a_2^2}\right) E\left(d + a_1 + a_2 + a_1\sqrt{1-r^2/a_1^2} + a_2\sqrt{1-r^2/a_2^2}\right) r \, \mathrm{d}r \,, \tag{A16}$$

where E is the interaction energy per unit area between two infinite flat plates separated by a distance h and is expressed by Eqs. (3) and (4) for VDW and EDL interactions, respectively.

Appendix B

Ohshima [57] developed a very useful analytical equation to accurately estimate $f(\kappa a)$ as a function of the particle size and Debye length:

$$f(\kappa a) = 1 + \frac{1}{2(1+\delta/\kappa a)^3}, \tag{B1}$$

where δ can be described by:

$$\delta = \frac{2.5}{1+2e^{-\kappa a}}. \tag{B2}$$

The internal conductivity of the particle, σ_p, can be estimated using the so-called differential self-consistent model applied for disk-shaped particles [61, 63]:

$$\sigma_p = \frac{\sigma_b}{F}\left[F\Theta + \frac{1}{2}(1-\Theta)\left(1-\Theta+\sqrt{(1-\Theta)^2+4F\Theta}\right)\right], \tag{B3}$$

$$\Theta = \frac{\sigma_e}{\sigma_b} = \frac{2\Sigma_s}{a_e\sigma_b}, \tag{B4}$$

$$F = \phi^{-2}, \tag{B5}$$

where a_e is the radius of elementary NP and ϕ is the intra-aggregate porosity. Eq. (B3) has the advantage of not being restricted to any κa_e values.

The electrical conductivity of bulk water, σ_b, is calculated by:

$$\sigma_b = \sum_{i=1}^{N} e 1000 N_A z_i \beta_i^b c_i^b, \tag{B6}$$

where N is the number of types of ions and β_i^b is the ionic mobility in bulk water (in m^2 s^{-1} V^{-1}).

The specific surface conductivity, Σ_s, due to the electromigration of counter-ions in the Stern layer and to the electromigration of hydrated counter-ions and co-ions in the

diffuse layer, can be calculated as a function of pH and salinity using Revil and Glover's electrokinetic transport model [60]:

$$\Sigma_s = \sum_i z_i e \beta_i^{\mathrm{St}} \Gamma_i^{\mathrm{St}} + 2\kappa^{-1} e 1000 N_A z \left\{ \left(c_{(+)}^b B_{(+)} + c_{\mathrm{H}^+}^b B_{\mathrm{H}^+} \right) \left[\exp\left(\frac{-ez\psi_d}{2k_b T} \right) - 1 \right] \right.$$

$$\left. + \left(c_{(-)}^b B_{(-)} + c_{\mathrm{OH}^-}^b B_{\mathrm{OH}^-} \right) \left[\exp\left(\frac{ez\psi_d}{2k_b T} \right) - 1 \right] \right\}, \quad \text{(B7)}$$

$$B_i = \beta_i^b + \frac{2\varepsilon_0 \varepsilon_r k_b T}{\eta e z_i}, \quad \text{(B8)}$$

where β_i^{St} is the ionic mobility of adsorbed counter-ions at the Stern layer (in $m^2\ s^{-1}\ V^{-1}$), Γ_i^{St} is their surface site density (in sites m^{-2}), and "+" and "–" stand for cations and anions, respectively. As shown in Eq. (B7), the specific surface conductivity, Σ_s, depends on the surface site density of adsorbed counter-ions at the Stern layer, Γ_i^{St}, and on the electrostatic potential at the OHP, ψ_d. Γ_i^{St} and ψ_d can be calculated using an extended Stern model (ESM, Fig. 3), which describes the electrochemical properties of the TiO_2/water interface [8, 18].

Figure captions

Fig. 1. Two interacting spherical particles with radii a_1 and a_2. The centers of the spheres are origins of two body-fixed coordinate systems, with their *z* axes directly facing each other. The *xy* planes of these coordinate systems are parallel to each other (from Bhattacharjee et al. [51]).

Fig. 2. Effect of the electrical double layer around the particle on the applied electrical field. Non-conducting particles (**a.**) and conducting particles (**b.**) (from Lyklema and Minor [55]). Du is the Dukhin number, which is defined as half the ratio of surface electrical conductivity to bulk electrical conductivity.

Fig. 3. The simplified sketch of the extended Stern model (ESM) of Leroy et al. [18]. M^+ are metal cations (e.g., Na^+ or K^+) and A^- are anions (e.g., Cl^-). OHP is the outer Helmholtz plane, which corresponds here to the shear plane where the zeta potential (ζ) is defined. *Q* is the surface charge density of the three different layers (mineral surface, Q_0, Stern, Q_β, and diffuse layer, Q_d). *C* is the capacitance between the "0-plane" and the "β-plane" (C_1), and between the "β-plane" and the "*d*-plane" (C_2).

Fig. 4. "Observed" zeta potentials of pure TiO_2 NPs versus pH at 10^{-4}, 10^{-3}, and 10^{-2} M KCl from Snoswell et al. [22] (**a**; squares) and calculated using the approach of Leroy et al. [18] (**b**; circles). The curves are the ESM predictions assuming $\psi_d = \zeta$ [18].

Fig. 5. The predicted Dukhin numbers of (**a**) an elementary NP and (**b**) an aggregate versus pH at 10^{-4}, 10^{-3}, and 10^{-2} M KCl. The mean radius of elementary NPs is equal to 6 nm ([22]), and the radius of the aggregate is optimized by decreasing the cost function $R^2 = \sum_{i=1}^{L} \left[\zeta_{\text{obs}}(i) - \psi_d(i)\right]^2$ using the Simplex algorithm [66] (where *L* is the number of experimental values). The intra-aggregate porosity is equal to 10 %.

Fig. 6. The aggregation behavior of two nanoparticles (**a**) and of two aggregates (**b**) showing that stability is determined by the two nanoparticles involved if the range of interaction (defined by the thickness of the diffuse layer) is largely inferior to their size (from Schwarzer and Peukert [69]).

Fig. 7. Stability ratios versus salinity (KCl) (in log scale) at three different pH values (pH = 6.3, 6.7, and 8.4). Experimental data from Snoswell et al. [22] (squares) and model predictions with DA (solid lines) and SEI (dotted lines). Two cases are considered: the effective interaction radius is constant with pH (**a**) and the effective interaction radius varies with pH (**b**).

Fig. 8. Interaction energy profiles calculated by DA (solid lines) and SEI (dotted lines) at three different pH values (pH = 6.3, 6.7, and 8.4) and in the case of a constant effective interaction radius. **a.** Salinity of 10^{-2} M KCl. **b.** Salinity of $10^{-1.5}$ M KCl.

References

[1] M.R. Wiesner, G.V. Lowry, P. Alvarez, D. Dionysiou, P. Biswas, Environ. Sci. Technol. 40 (2006) 4336.

[2] A.R. Petosa, D.P. Jaisi, I.R. Quevedo, M. Elimelech, N. Tufenkji, Environ. Sci. Technol. 44 (2010) 6532.

[3] H.F. Lecoanet, J.Y. Bottero, M.R. Wiesner, Environ. Sci. Technol. 38 (2004) 5164.

[4] B. Nowack, T.D. Bucheli, Environ. Pollut. 150 (2007) 5.

[5] P. Biswas, C.Y. Wu, J. Air Waste Manage. 55 (2005) 708.

[6] H.F. Lecoanet, M.R. Wiesner, Environ. Sci. Technol. 38 (2004) 4377.

[7] K.A.D. Guzman, M.P. Finnegan, J.F. Banfield, Environ. Sci. Technol. 40 (2006) 7688.

[8] G.D. Panagiotou, T. Petsi, K. Bourikas, C.S. Garoufalis, A. Tsevis, N. Spanos, C. Kordulis, A. Lycourghiotis, Adv. Colloid Interface Sci. 142 (2008) 20.

[9] K. Bourikas, T. Hiemstra, W. Van Riemsdijk, Langmuir (2001) 749.

[10] X.Y. Liu, G.X. Chen, C.M. Su, J. Colloid Interface Sci. 363 (2011) 84.

[11] R.A. French, A.R. Jacobson, B. Kim, S.L. Isley, R.L. Penn, P.C. Baveye, Environ. Sci. Technol. 43 (2009) 1354.

[12] Y. Zhang, Y.S. Chen, P. Westerhoff, J. Crittenden, Water. Res. 43 (2009) 4249.

[13] J.M. Herrmann, Catal. Today 53 (1999) 115.

[14] M.R. Hoffmann, S.T. Martin, W.Y. Choi, D.W. Bahnemann, Chem. Rev. 95 (1995) 69.

[15] E.M. Hotze, T. Phenrat, G.V. Lowry, J. Environ. Qual. 39 (2010) 1909.

[16] M. Elimelech, J. Gregory, X. Jia, R.A. Williams, Butterworth-Heinemann, Boston, 1995, 448p.

[17] N. Solovitch, J. Labille, J. Rose, P. Chaurand, D. Borschneck, M.R. Wiesner, J.Y. Bottero, Environ. Sci. Technol. 44 (2010) 4897.

[18] P. Leroy, C. Tournassat, M. Bizi, J. Colloid Interface Sci. 356 (2011) 442.

[19] J. Lyklema, Academic Press, London, 1991, 736p.

[20] J.J. Bikerman, Trans. Faraday Soc. 35 (1940) 154.

[21] A. Crespy, A. Boleve, A. Revil, J. Colloid Interface Sci. (2007) 188.

[22] D.R.E. Snoswell, J.M. Duan, D. Fornasiero, J. Ralston, Int. J. Miner. Process. 78 (2005) 1.

[23] I. Larson, C.J. Drummond, D.Y.C. Chan, F. Grieser, J. Am. Chem. Soc. 115 (1993) 11885.

[24] H.D. Ackler, R.H. French, Y.M. Chiang, J. Colloid Interface Sci. 179 (1996) 460.

[25] M.K. Ridley, V.A. Hackley, M.L. Machesky, Langmuir 22 (2006) 10972.

[26] A.M. Puertas, F.J. de las Nieves, J. Colloid Interface Sci. 216 (1999) 221.

[27] E.J.W. Verwey, J.T.G. Overbeek, Elsevier, Amsterdam, 1948, 218p.

[28] B.V. Derjaguin, L. Landau, Acta Physicochim. USSR. 14 (1941) 633.

[29] H. Kihira, N. Ryde, E. Matijevic, Colloid Surf. 64 (1992) 317.

[30] N. Kallay, T. Preocanin, D. Kovacevic, Croat. Chem. Acta 82 (2009) 531.

[31] S.Y. Shulepov, J. Colloid Interface Sci. 189 (1997) 199.

[32] S.S. Dukhin, J. Lyklema, Langmuir 3 (1987) 94.

[33] G. Frens, J.T.G. Overbeek, J. Colloid Interface Sci. 38 (1972) 376.

[34] J. Israelachvili, H. Wennerstrom, Nature 379 (1996) 219.

[35] P. Kekicheff, O. Spalla, Phys. Rev. Lett. 75 (1995) 1851.

[36] S.Y. Shulepov, G. Frens, J. Colloid Interface Sci. 182 (1996) 388.

[37] S.H. Behrens, D.I. Christl, R. Emmerzael, P. Schurtenberger, M. Borkovec, Langmuir 16 (2000) 2566.

[38] M. Elimelech, C.R. O'Melia, Langmuir 6 (1990) 1153.

[39] N. Kallay, M. Colic, D.W. Fuerstenau, H.M. Jang, E. Matijevic, Colloid Polym. Sci. 272 (1994) 554.

[40] R. Hogg, T.W. Healy, D.W. Fuerstenau, Trans. Faraday Soc. 62 (1966) 1638.

[41] N. Kallay, S. Zalac, J. Colloid Interface Sci. 253 (2002) 70.

[42] W. Zhang, J. Crittenden, K.G. Li, Y.S. Chen, Environ. Sci. Technol. 46 (2012) 7054.

[43] E.P. Honig, G.J. Roebersen, P.H. Wiersema, J. Colloid Interface Sci. 36 (1971) 97.

[44] R.J. Hunter, Academic Press, New York, 1981, 386p.

[45] H.C. Hamaker, Physica 4 (1937) 1058.

[46] G. Frens, Dissertation, Utrecht, 1968, 88p.

[47] G.M. Bell, S. Levine, L.N. McCartney, J. Colloid Interface Sci. 33 (1970) 335.

[48] D. Leckband, J. Israelachvili, Q. Rev. Biophys. 34 (2001) 105.

[49] J. Gregory, J. Colloid Interface Sci. 51 (1975) 44.

[50] S.L. Carnie, D.Y.C. Chan, J. Stankovich, J. Colloid Interface Sci. 165 (1994) 116.

[51] S. Bhattacharjee, M. Elimelech, M. Borkovec, Croat. Chem. Acta 71 (1998) 883.

[52] S. Bhattacharjee, A. Sharma, Langmuir 12 (1996) 5498.

[53] S. Bhattacharjee, M. Elimelech, J. Colloid Interface Sci. 193 (1997) 273.

[54] D.C. Henry, Proc. R. Soc. Lond. A 133 (1931) 106.

[55] J. Lyklema, M. Minor, Colloids Surf. A: Physicochem. Eng. Asp. 140 (1998) 33.

[56] D.C. Henry, Trans. Faraday Soc. 44 (1948) 1021.

[57] H. Ohshima, J. Colloid Interface Sci. 168 (1994) 269.

[58] E. Hückel, Physikalische Zeitschrift 25 (1924) 204.

[59] M. Von Smoluchowski, L. Graetz, Leipzig, 1921, 385p.

[60] A. Revil, P. Glover, Geophys. Res. Lett. (1998) 691.

[61] P.N. Sen, C. Scala, M.H. Cohen, Geophysics 46 (1981) 781.

[62] A. Revil, P.W.J. Glover, Phys. Rev. B 55 (1997) 1757.

[63] A. Revil, J. Geophys. Res.-Sol. Ea. 105 (2000) 16749.

[64] S.S. Dukhin, V.N. Shilov, Wiley & Sons Incorporated John, New York, 1974, 192p.

[65] D.L. Parkhurst, C.A.J. Appelo, U.S. Geological Survey Water-Resources Investigations Report, 1999, 312p.

[66] M. Caceci, W.P. Cacheris, Byte 9 (1984) 340.

[67] L. Bergstrom, Adv. Colloid Interface Sci. 70 (1997) 125.

[68] T. Hiemstra, W.H. Van Riemsdijk, J. Colloid Interface Sci. 301 (2006) 1.

[69] H.C. Schwarzer, W. Peukert, Chem. Eng. Sci. 60 (2005) 11.

[70] S. Biggs, KONA 24 (2006) 41.

[71] B. Gilbert, G.P. Lu, C.S. Kim, J. Colloid Interface Sci. 313 (2007) 152.

Table 1. Optimized parameters of our aggregation kinetics model (constant effective interaction radius).

Parameters	DA	SEI
$d_{\min}$ nm	3.4 ± 1	4 ± 1
A_{H} 10^{-20} J	5.89 ± 0.2	7.68 ± 0.2
a_i nm	16.12 ± 1	28.68 ± 1
R^2	0.63	1.48

Table 2. Optimized parameters of our aggregation kinetics model (variable effective interaction radius; distances are expressed in nm).

Parameters	DA	SEI	DA	SEI
$d_{\min}$	2.4 ± 1	2.7 ± 1	1.66	1.66
$A_{\mathrm{H}}\ 10^{-20}\,\mathrm{J}$	6.81 ± 0.2	8.32 ± 0.2	7.13 ± 0.2	8.71 ± 0.2
a_i (pH = 6.3)	31.80 ± 1	65.44 ± 1	33.71 ± 1	67.87 ± 1
a_i (pH = 6.7)	17.82 ± 1	29.36 ± 1	19.08 ± 1	30.91 ± 1
a_i (pH = 8.4)	8.99 ± 1	12.35 ± 1	5.76 ± 1	7.97 ± 1
R^2	0.11	0.13	0.17	0.23